Acta Geotechnica (2020) 15:615–633
https://doi.org/10.1007/s11440-018-00761-y

RESEARCH PAPER

# Influence of matric suction on nonlinear time-dependent compression behavior of a granular fill material

Wen-Bo Chen[1] · Kai Liu[1] · Wei-Qiang Feng[1] · Lalit Borana[2] · Jian-Hua Yin[1,3]

Received: 5 March 2018 / Accepted: 27 December 2018 / Published online: 23 January 2019


**Abstract**
The site formation for the construction of a new airport in a mountainous region is typically performed by cutting and filling a hill section. The fill materials are subjected to seasonal changes and large variations in water content. The water content change renders the fill material to be characterized as unsaturated or saturated. This study aims to investigate the influence of matric suction on the time-dependent compression behavior of one local soil as a fill material for the construction of a new runway of an airport in Chongqing city, a mountainous region in China. A series of unsaturated drained triaxial tests were conducted on this coarse-grained soil to obtain the relationship between the effective stress parameter, $\chi$, and the matric suction. Subsequently, multistaged compression tests were performed on this soil using a newly designed suction-controlled oedometer apparatus. The influence of suction on the time-dependent compression behavior of the fill material is emphasized. The results indicate that the matric suction can increase the compression stiffness, and that the unloading–reloading index varies nonlinearly with suction. A linear relationship between the time-dependent compression coefficient and normalized effective vertical loading is established. The linear relationship is subsequently used to predict the time-dependent compression coefficient to describe the time-dependent behavior of the fill under unsaturated conditions. Further, a nonlinear function based on the work of Yin (Géotechnique 49(5):699–707, 1999) is adopted to describe the development of time-dependent compression. The results indicate that the prediction obtained from the two newly proposed methods are promising, and can predict the nonlinear time-dependent compression behavior of this coarse-grained soil.

**Keywords** Compressibility · Creep · Fill · High embankment · Oedometer · Suction · Time dependent

## 1 Introduction

In recent years, the Chinese aviation industry has progressed rapidly to cater to the demands of the fast movement of people and goods. These demands require the construction of new airports, particularly in hilly terrains. The majority of territorial areas in Mainland China (approximately 70%) are mountainous regions. The airport development in the mountainous areas of Mainland China is of considerable strategic importance to the social and economic establishments of the country. The construction of an airfield in such terrain with highly variable elevation involves large volumes of earth fills that form the high

✉ Jian-Hua Yin
cejhyin@polyu.edu.hk

Wen-Bo Chen
geocwb@gmail.com

Kai Liu
kevin-kai.liu@connect.polyu.hk

Wei-Qiang Feng
wqfeng@polyu.edu.hk

Lalit Borana
lalitborana@gmail.com

[1] Department of Civil and Environmental Engineering, The Hong Kong Polytechnic University, Hung Hom, Kowloon, Hong Kong, China

[2] Department of Civil Engineering, Indian Institute of Technology Indore, Simrol, Indore, India

[3] PolyU Shenzhen Research Institute, Shenzhen, China

embankments. The maximum height of these embankments can reach 100 m at some locations [62]. The large self-weight of fill materials can cause excessive settlement of the embankment in both the construction and post-construction periods. For the environmental and financial concerns, a balance between filling and cutting is often preferred. Therefore, in many cases, local soils that might exhibit poor engineering properties are often utilized as fill materials, as it is a viable option. The fill materials typically contain large granular particles, and the water in the pores can easily drain out, thereby resulting in a partially saturated state of the soil. Owing to the seasonal variations (such as precipitation and temperature), the soil water content and settlement behavior of the embankments are affected significantly.

The horizontal and vertical movements of a rockfill dam are affected significantly by the first-time reservoir filling and heavy rainfall [37, 38]. The investigation for examining the effect of matric suction on reconstituted soils revealed that the preconsolidation stress ($\sigma_{vp}$) increases with matric suction. Mountassir et al. [45] examined the influence of compaction conditions, such as dry density and initial water content, on the collapsible behavior of a flood defense embankment soil. The results indicated that regardless of the level of dry density, the specimens were insensitive to the change in water content if the specimen is compacted at the optimum or wet of optimum soil moisture content. In contrast, the collapsible behavior of silty sand [50] or lumpy soils [53, 57, 58] on wetting is prudent even if the compaction of the specimen is achieved at the optimum water content. Furthermore, the findings demonstrate that the matric suction has a significant influence on the compressibility, stiffness and shear strength parameters of soil.

The compression of soils under a certain loading is typically highly nonlinear with time. However, at the microscopic level, the mechanisms of the time-dependent compression of cohesive soils and cohesionless soils are different. For cohesive soils, the primary influencing factors are the absorbed water system, viscosity, and physicochemical properties of the clay–water system [33, 67]. However, for cohesionless soils, inter-particle slip, rotation, crushing, or even fracturing and splitting lead to the time-dependent compression [14, 15, 16, 24, 37]. Mesri and Vardhanabhuti [43] stated that close packing of particles is a locking process, while slip and fracturing are unlocking processes. These two processes alternate to become more dominant or achieve a balance between each other during the entire compression period.

Oldecop and Alonso [48] reported that the post-construction settlement of rockfill dams might continue to accumulate even after 10–30 years of service. The test results indicate that the ratio between the time-dependent compression coefficient and the compression index remained approximately constant at a value 0.02, except for the specimens in an very dry condition. Oldecop and Alonso [48] defined the compression index as follows:

$$\lambda = \frac{\mathrm{d}(\varepsilon)}{\mathrm{d}(\ln \sigma_{\mathrm{v}})} \tag{1}$$

where $\lambda$ is the compression index, $\mathrm{d}(\varepsilon)$ is the strain increment and $\sigma_{\mathrm{v}}$ is the total vertical stress applied on the specimen. Further, the time-dependent compression coefficient is expressed as follows:

$$\lambda^{t} = \frac{\mathrm{d}(\varepsilon)}{\mathrm{d}(\ln t)} \tag{2}$$

where $\mathrm{d}(\varepsilon)$ is the strain increment, and $t$ is the time elapsed since adding the load. It is noteworthy that the parameter "$\lambda$" and "$\lambda^{t}$" are different from the "$\lambda$" in the Cam-Clay model [11] and the creep coefficient "$\psi$" in the one-dimensional elastic viscoplastic (EVP) model in one-dimensional condition [65, 66]. Based on the investigations by Mcdowell and Bolton [40] and Oldecop and Alonso [47], the compression process is divided into two parts. The first part is clastic yielding (CY), in which the compression index increases linearly with the applied stress. The second part is clastic hardening (CH), during which the compression index maintains approximately constant. A model describing the time-dependent strain under constant stress and matric suction was proposed by Oldecop and Alonso [47]:

$$\text{during CY}: \varepsilon \cong \lambda\left[\left(\frac{t}{t^{r}}\right)^{1/n} - 1\right] + \varepsilon_{0} \tag{3}$$

$$\text{during CH}: \varepsilon \cong \frac{\lambda}{n}\ln\left(\frac{t}{t^{r}}\right) + \varepsilon_{0} \tag{4}$$

where $t$ is the time elapsed since the application of the total vertical load; $\varepsilon$ is the strain at time $t$; $t^{\mathrm{r}}$ is the reference time; $n$ is a constant that represents the ratio of the creep coefficient and compression index; $\varepsilon_0$ is the strain at $t^{\mathrm{r}}$. The present study also aims to evaluate the prediction performance of this model. It is noteworthy that in this study, the change in specimen compression deformation is expressed by the change in void ratio ($\Delta e = e - e_0$). Therefore, the compression index and the time-dependent compression coefficient are denoted as $C_c$ and $C_t$, respectively. Moreover, the relationship between $\Delta\varepsilon$ ($\Delta\varepsilon = \varepsilon - \varepsilon_0$) and $\Delta e$ can be expressed as follows:

$$\Delta\varepsilon = -\frac{\Delta e}{1 + e_0} \tag{5}$$

where $e_0$ is the initial void ratio of the specimen.

The selection of stress state variables is crucial in describing the soil behavior. However, no complete

consensus on this issue for unsaturated soil has been reached [29, 30, 51]. It is noteworthy that, in Eq. (1), the compression index is calculated based on the total vertical stress ($\sigma_v$). Bishop [4], and Bishop and Blight [5] proposed a classical expression of the effective stress for unsaturated soils, expressed as follows:

$$\sigma' = (\sigma - u_a) + \chi(u_a - u_w) \quad (6)$$

where $\sigma'$, $\sigma$, $u_a$, and $u_w$ are the effective stress, total stress, pore air pressure, and pore water pressure, respectively, $\chi$ is an effective stress parameter related to the saturation degree ($S_r$) or matric suction ($s$) of soil. $\chi$ can be defined from thermodynamics [9] or from experimentally [4, 5, 29]. The arguments against the single parameter of $\sigma'$ are primarily the following: (a) it cannot explain the collapse phenomenon of soils upon wetting; (b) no unique relationship between $\chi$ and the degree of saturation or matric suction can be established. Fredlund and Morgenstern [19] suggested that any two of the three stress parameters $\sigma - u_a$, $\sigma - u_w$, $u_a - u_w$ would be sufficient to well capture the stress state of unsaturated soils. Khalili et al. [30] argued that $u_a - u_w$ is a stress variable in the pore scale, which is contrasted with the typical approach in continuum mechanics, in which the stress variables are averaged over the element behavior. Therefore, they concluded that the mixing of scales can lead to complex constitutive modeling with intractable stress–strain relationships. In this study, the single stress variable of effective stress is adopted.

Feeble attempts have been performed to study the compression and time-dependent compression behavior of soils in suction-controlled conditions. Most investigations have focused primarily on soils with relatively single gradation, such as sand, clay, and rockfill, under completely saturated or dry conditions. The literature review also suggests insufficiency in examining the settlement behavior of a poorly graded soil consisting of a mixture of soils and rocks. It is noteworthy that the structure of rock–soil mixtures is analogous to that of lumpy composite soils [55]. A unique homogenization law [54] and a constitutive modeling [56, 57] were proposed for capturing the deformation behavior of lumpy composite soil. This provides a possible reference for analyzing the deformation of poorly graded coarse-grained soil. However, these theoretical modeling cannot consider the effect of water content or matric suction change. Therefore, the investigation on the coupling effect of the high-stress level, and matric suction on the behavior of the fill material would be helpful to understand the compression mechanism of coarse-grained soils, and provide guidance for the engineering practice.

In this study, a poorly graded coarse-grained soil is adopted as the testing material. A series of unsaturated triaxial tests were conducted to determine the relationship between the effective stress parameter and matric suction. Subsequently, a new suction-controlled oedometer device was designed, manufactured and employed to conduct unsaturated oedometer tests to investigate the compression behavior. The test results were subsequently used to modify an existing model and validate a nonlinear function. Furthermore, the results obtained experimentally were analyzed and discussed.

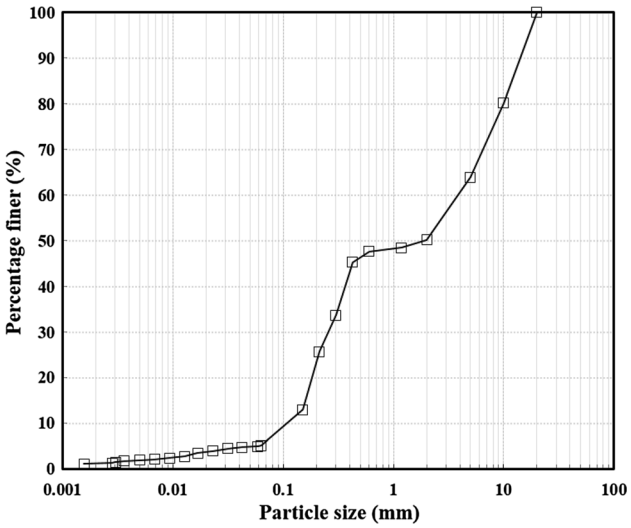


**Fig. 1** Particle size distribution curve of the tested fill

## 2 Materials, apparatus, and testing scheme

### 2.1 Soil

The soil utilized for testing in this study is a fill material, that is adopted in the high-filled embankment of an airport. The soil is dull red and is classified as poorly graded gravel with sand [1]. It is noteworthy that for testing purposes, all particles larger than 20 mm in diameter were removed by sieving. Figure 1 shows the particle size distribution curve of the tested fill material after scaling. The coefficient of curvature is 0.138, and the coefficient of uniformity is 35.47. The scaled-down soil was first divided into eight groups characterized by eight particle size ranges: 10–20 mm, 5–10 mm, 2–5 mm, 0.3–2 mm, 0.212–0.3 mm, 0.15–0.212 mm, 0.063–0.15 mm, and $< 0.063$ mm. The photographs of the typical particles in four different size ranges are shown in Fig. 2. The soil possesses a specific gravity of 2.73 and has a maximum dry density value of 2.12 Mg/m$^3$ at an optimum moisture content of 5.7% [10]. Figure 3 shows the soil–water characteristic curve (SWCC) obtained by the filter paper

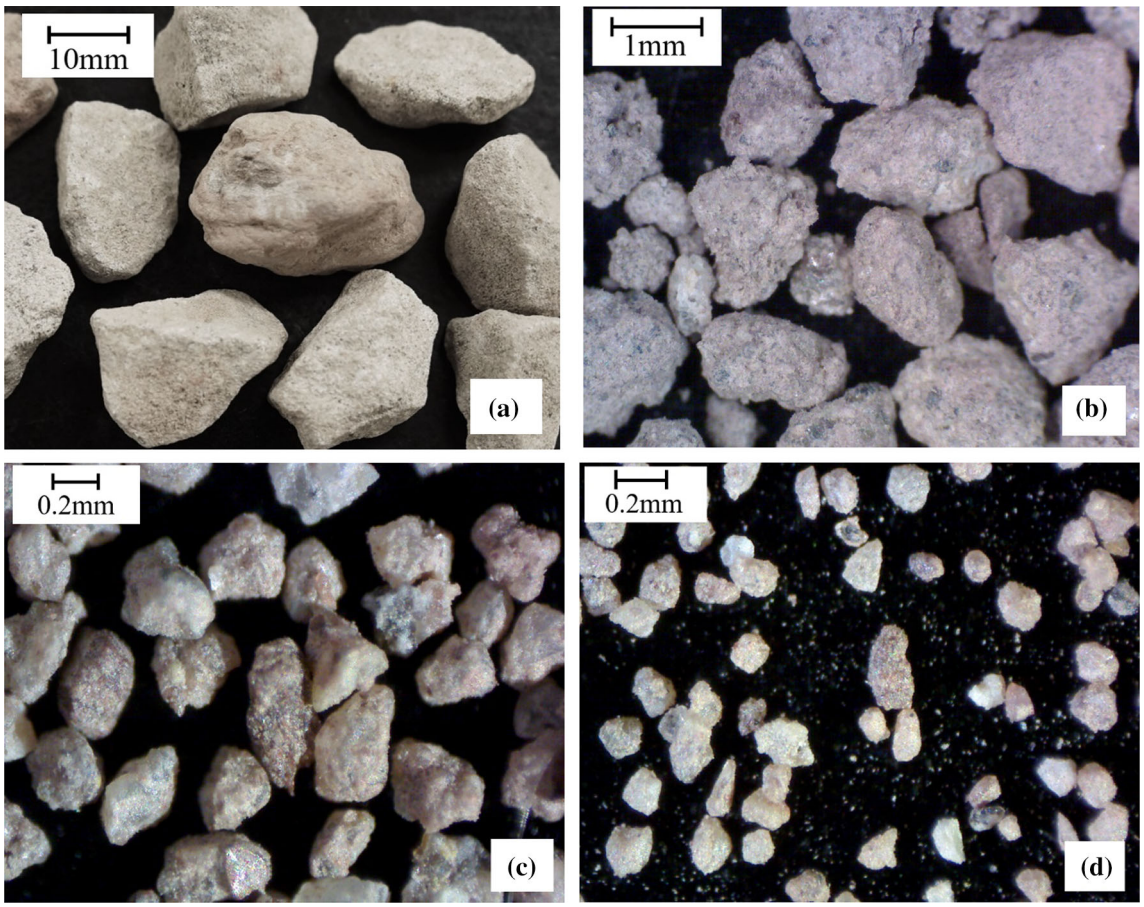


**Fig. 2** The photos of typical soil particles of fill material in the size ranges of **a** 10–20 mm; **b** 0.3–2 mm; **c** 0.212–0.3 mm; **d** 0.063–0.212 mm

method [2], and the fitting curve using the Fredlund and Xing model [20, 49].

## 2.2 Test apparatuses

The axis translation technique is a popular and precise method to control the matric suction [6, 69]; hence, it was adopted for this study.

Figure 4 depicts the schematic diagram of the newly designed oedometer apparatus. The apparatus utilized in this study is an improved version of the Modified Direct Shear Apparatus (MDSA) described by Borana et al. [7, 8]. Therefore, in the air chamber, two lateral loading pistons were used for the direct shear test, as shown in figure. A stainless-steel ring of height 140 mm and internal diameter 100 mm was positioned inside the air chamber. The inner wall of this ring was polished carefully to reduce friction. A bottom platen was enclosed with a High Air Entry Value Ceramic Disk (HAEVCD). It also accommodates the water chamber, that was located below the HAEVCD. During testing, the top platen (99 mm in diameter) was placed on top of the soil specimen. Air pressure was applied to the soil specimen through the air vent and the gap around the top platen. The loading ram was positioned centrally over the top platen. The high-density polyurethane (HDPE)

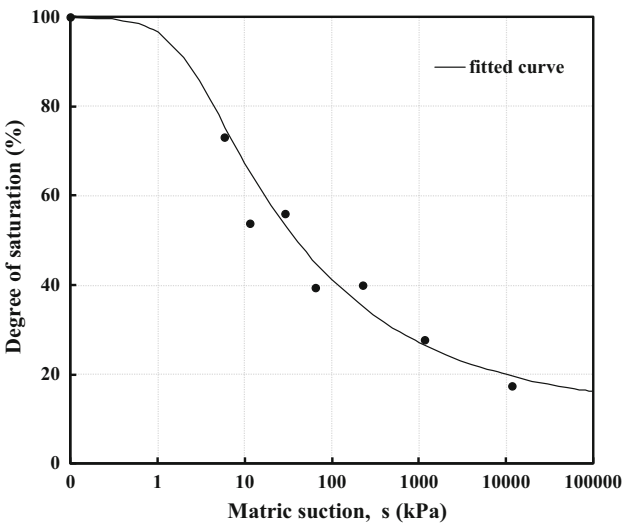


**Fig. 3** The soil–water characteristic curve (SWCC) of the tested fill

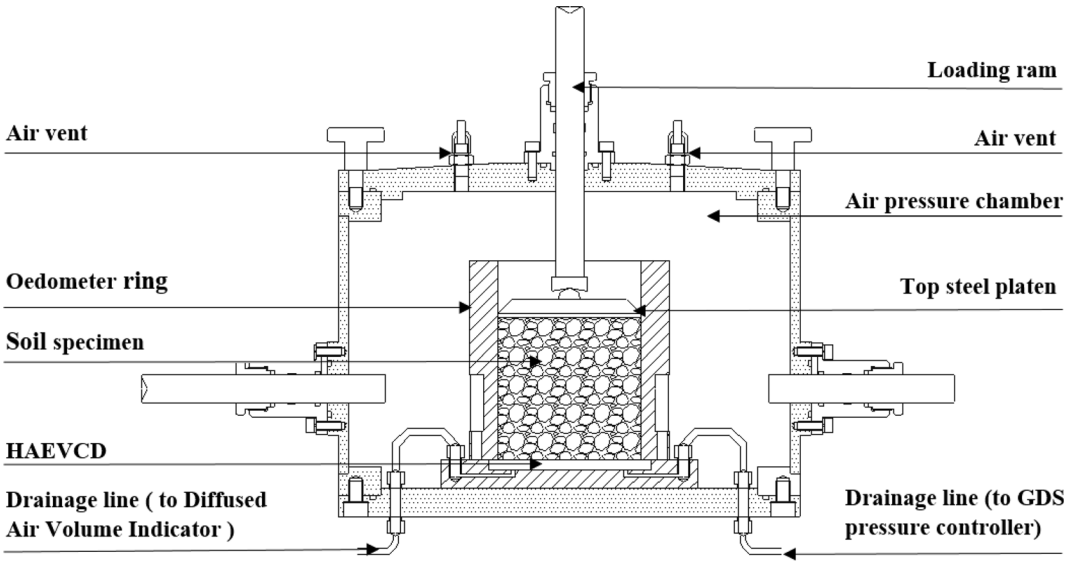


**Fig. 4** A schematic diagram of the newly designed suction-controlled oedometer apparatus

drainage cable was 4 mm in diameter, and connected to the diffused air volume indicator and GDS pressure controller. The auto volume change (AVC) device was connected to the water chamber via the HDPE cable. Lever-amplified dead weight was used to apply the target vertical load on the specimen. All the components of the testing devices, such as the pressure transducers and linear variable differential transducers (LVDTs), were connected to the data logger and computer.

Figure 5 shows the double-cell triaxial system used for the unsaturated consolidated drained triaxial tests. The details of this system were introduced systematically by Chen et al. [13].

## 2.3 Test procedures of unsaturated oedometer test

All the preliminary preparations, such as leakage inspection, saturation of ceramic disk, and calibration of different components of the testing devices, were performed before commencing the experimental testing by following the guidelines presented by Borana et al. [6].

Before the compaction of the soil specimen, a thin film of silicone gel was smeared evenly on the inner wall of the ring. According to the particle distribution curve shown in Fig. 1, the predetermined mass of each group size was weighted and mixed together. Subsequently, the soil was mixed with water to the optimum water content and matured for at least 24 h, following which it was compacted using a rotary hammer in five layers. Each soil layer was compacted to achieve a 20-mm height and a target dry density of 1.87 Mg/m$^3$ (88% of MDD). After placing each layer, the surface of the layers was scratched to ensure proper bonding between the subsequent soil layers. After the completion of the compaction process, the soil specimen was submerged in distilled water with sufficient water on the top surface. The oedometer cell was placed in the air chamber, and a constant vacuum pressure of 5 kPa was applied through the air vent for at least 12 h. This process facilitated the saturation process without disturbing the soil fabric of the specimen. After achieving saturation, the soil was subjected to equilibration for a target matric suction by controlling the predetermined air pressure and water pressure. The water pressure was maintained constant at 5 kPa for all the tests. The equilibration was presumed to be completed when the water content change was lower than 0.04%/day [26, 61]. This value is 0.587 ml/day in this study. Vertical stresses were applied to the specimen using a lever-amplified dead weight and by considering all the necessary load corrections. The vertical loading was applied to the specimen only after ensuring that the specimen had achieved the equilibration of matric suction.

Step-wise increasing total vertical stresses were applied on the specimen in a prescribed sequence as listed in Table 1. It is noteworthy that the effective vertical stress ($\sigma_v'$) is not presented in Table 1, and it can be calculated using $\chi$ and Eq. (6). The details of obtaining $\chi$ will be introduced in later sections. All the durations of loading are at least 12 h, and at least 48 h for the loadings for investigating the time-dependent compression behavior. If the unit weight of fill material is assumed as approximately 17 kN/m$^3$, the simulated height is approximately 60–80 m. Two unloading–reloading loops exist for every specimen. The air pressure and water pressure in the chambers were maintained constant during the test. To monitor the

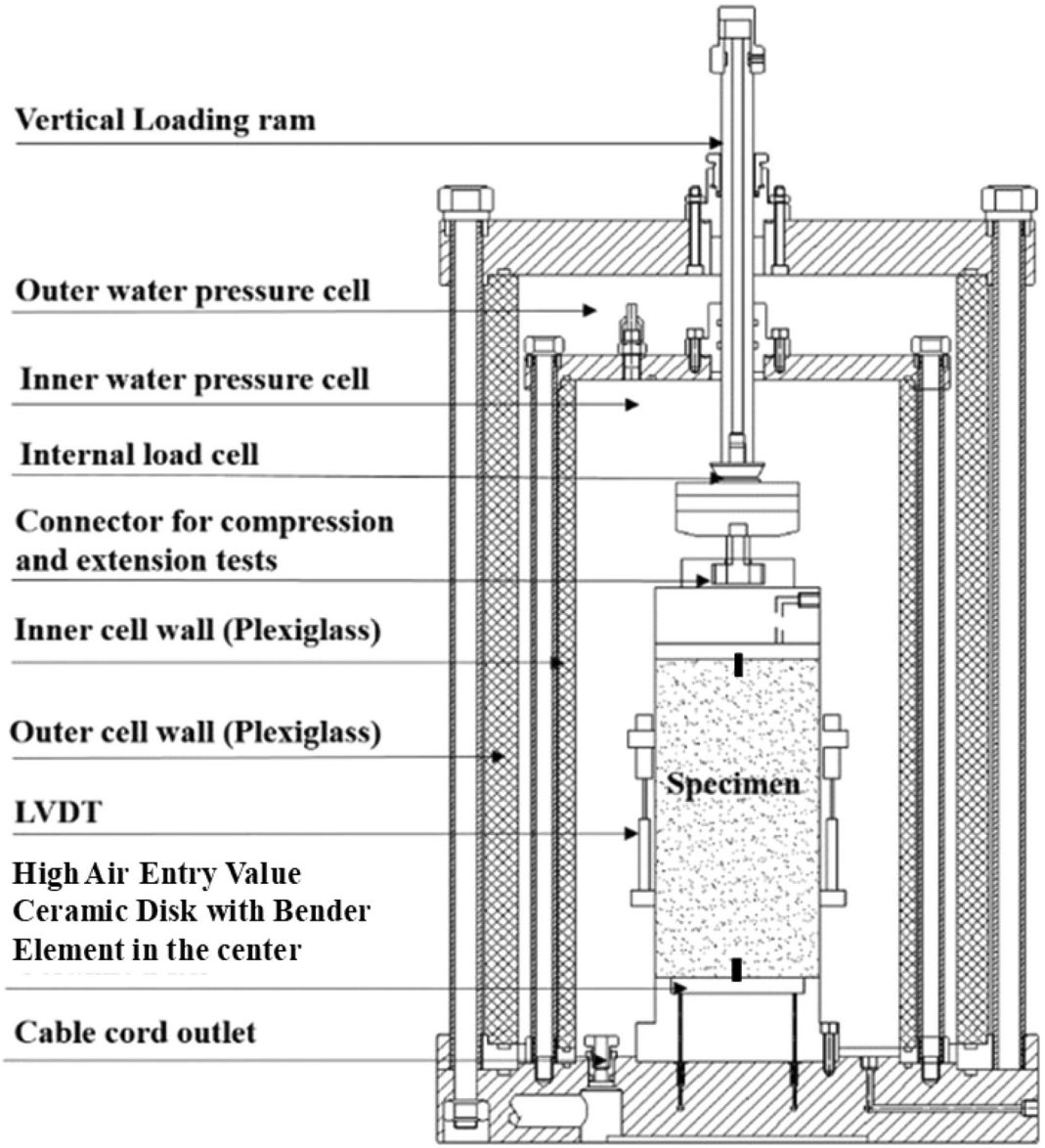


**Fig. 5** A schematic diagram of the newly designed suction-controlled double-cell triaxial apparatus (after Chen et al. [13])

dissipation of excess pore water pressure owing to stress change, the draining-out rate of water from the specimen was monitored by calculating the readings of the AVC that was connected to the water chamber. Typically, this re-equilibration stage (primary consolidation) lasted for 2–3 h. This implies that, for the tested soil, the excess pore water pressure does not build up obviously owing to the stress increment.

## 2.4 Test procedures of drained triaxial test

The soil treatment for the triaxial specimen is the same as that described in the last section. The triaxial specimens were 100 mm in diameter and 200 mm in height. The

**Table 1** Test scheme for unsaturated consolidated drained triaxial tests

| Test no. | $\sigma_a$ (kPa) | $\sigma_w$ (kPa) | $s$ (kPa) | $\sigma - \sigma_a$ (kPa) |
|---|---|---|---|---|
| 1 | 0 | 0 | 0 | 150 |
| 2 | 0 | 0 | 0 | 300 |
| 3 | 0 | 0 | 0 | 450 |
| 4 | 85 | 5 | 80 | 150 |
| 5 | 165 | 5 | 160 | 150 |
| 6 | 45 | 5 | 40 | 450 |
| 7 | 85 | 5 | 80 | 450 |

specimens were compacted in five layers with 40 mm height for each layer. The dry density of each specimen was maintained the same as that for the oedometer test. Three saturated drained triaxial tests and four unsaturated drained triaxial tests were conducted. The test scheme of the drained triaxial test is listed in Table 2. The procedures of the unsaturated triaxial test follow those of Liu et al. [36]. First, the equalization of the matric suction was achieved for the specimen. Next, the cell pressure of the soil specimen was increased to a predetermined value, while the pore air pressure and pore water pressure were maintained constant. Finally, the specimen was sheared at a constant shearing rate of 0.004 mm/min to ensure the matric suction equilibrium throughout the soil specimen. The same shearing rate was used for the saturated tests to eliminate the effect of shearing rate on the strength.

## 3 Results and discussion

A series of suction-controlled triaxial and oedometer tests were performed on the coarse-grained soil under different stress states, to investigate the influence of matric suction on the compressibility behavior and time-dependent compression behavior of the soil. The selected test data, results, and observation are presented in the subsequent sections.

### 3.1 Effective stress parameter, $\chi$

The effective stress parameter, $\chi$, is 0 for very dry soils and 1 for saturated soils. Equation (6) well relates the total stress, pore air pressure and pore water pressure to the single stress variable (i.e., effective stress,$\sigma'$). In this study, the determination of the $\chi$ value follows the work of Khalili and Khabbaz [29], and Khalili et al. [30], whose studies have been validated extensively by the test data of other researchers, regardless of whether predicting the shear strength or volumetric strain of unsaturated soils [18, 23, 60, 61]. They proposed to determine the effective stress parameter $\chi$ as follows:

$$\chi = \frac{\tau - \tau_0}{(u_a - u_w)\tan\phi'} \tag{7}$$

where $\tau_0$ is the shear strength of the specimen in the saturated triaxial compression test, $\tau$ is the shear strength of the specimen under the same net mean stress $(\sigma - u_a)$ in the unsaturated triaxial compression test, and $\phi'$ is the effective internal friction angle, which is assumed to be constant for saturated and unsaturated specimens. Khalili and Khabbaz [29], and Khalili et al. [30] suggested a relationship between $\chi$ and the normalized matric suction, as expressed:

**Table 2** Test scheme for unsaturated oedometer tests

| Test no. | $\sigma_a$ (kPa) | $\sigma_w$ (kPa) | s (kPa) | $\chi$ | $\sigma_v$ (kPa) (arrows mean loading sequence) |
|---|---|---|---|---|---|
| 8 | 0 | 0 | 0 | 1 | 25 → 50 → 100 → 200* → 400 → 200 → 100 → 50 → 100 → 200 → 400 → 800* → 1000* → 800 → 400 → 200 → 400 → 800 → 1000 |
| 9 | 55 | 5 | 50 | 0.593 | 25 → 50 → 100 → 200 → 400* → 200 → 100 → 50 → 100 → 200 → 400 → 600 → 800* → 1000* → 800 → 600 → 400 → 800 → 1000 |
| 10 | 105 | 5 | 100 | 0.532 | 25 → 50 → 100 → 200* → 400 → 200 → 100 → 50 → 100 → 200 → 400 → 800* → 1200* → 800 → 400 → 200 → 400 → 800 → 1200 |
| 11 | 205 | 5 | 200 | 0.477 | 25 → 50 → 100 → 200 → 400* → 200 → 100 → 50 → 100 → 200 → 400 → 800* → 1400* → 800 → 400 → 200 → 400 → 800 → 1400 |

*Means this loading is kept for at least 48 h to investigate the time-dependent compression behavior

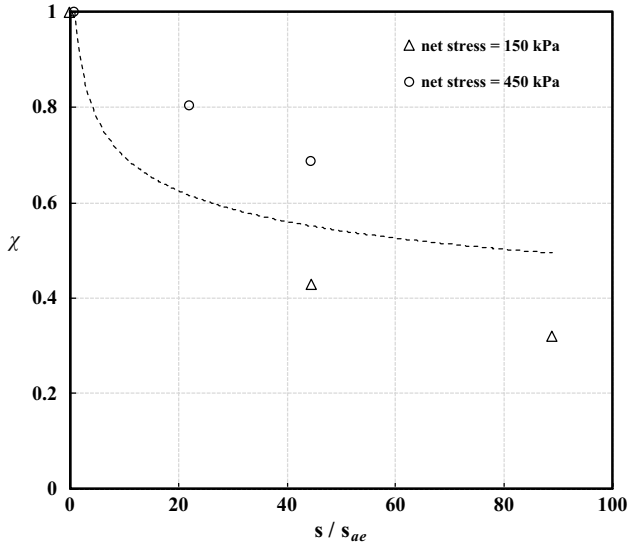


**Fig. 6** The relationship and fitting of effective stress parameter, $\chi$, versus normalized matric suction, $s/s_{ae}$

$$\chi = \left(\frac{s}{s_{ae}}\right)^{n} \tag{8}$$

where $s$ is the matric suction, $s_{ae}$ is the air entry value of the soil on the drying path, and $n$ is a fitting parameter. The matric suctions of all the tests in this study were equilibrated on the drying path such that only $s_{ae}$ (estimated as 1.8 kPa based the SWCC in Fig. 3) is determined as the reference for normalization. The effective internal friction angle, $\phi'$, is determined as 36.77° using the test data from the saturated triaxial tests. Figure 6 presents the relationship between the $\chi$ values of the saturated and unsaturated triaxial tests and the corresponding normalized matric suction ratio. The fitting parameter, $n$, is determined as − 0.157. Therefore, the $\chi$ value for each matric suction on the drying path can be determined. Table 2 lists the $\chi$ value calculated by the calibrated Eq. (8) for each oedometer test. It is noteworthy that the stress paths of the unsaturated tests in this study are all on the drying path such that the calibrated Eq. (8) is suitable for all the tests.

## 3.2 Compressibility behavior

Owing to the time-dependent compressibility characteristic of soil, the change in void ratio ($\Delta e$) discussed in this section refers to the total $\Delta e$ that occurred 12 h after the change in vertical stress.

The variations in the void ratio of the specimen under a 200 kPa matric suction versus time (logarithmic scale) are presented in Fig. 7. The vertical loadings in this figure are expressed in terms of the total vertical loading ($\sigma_v$). As expected, the void ratio decreases at a greater rate with an

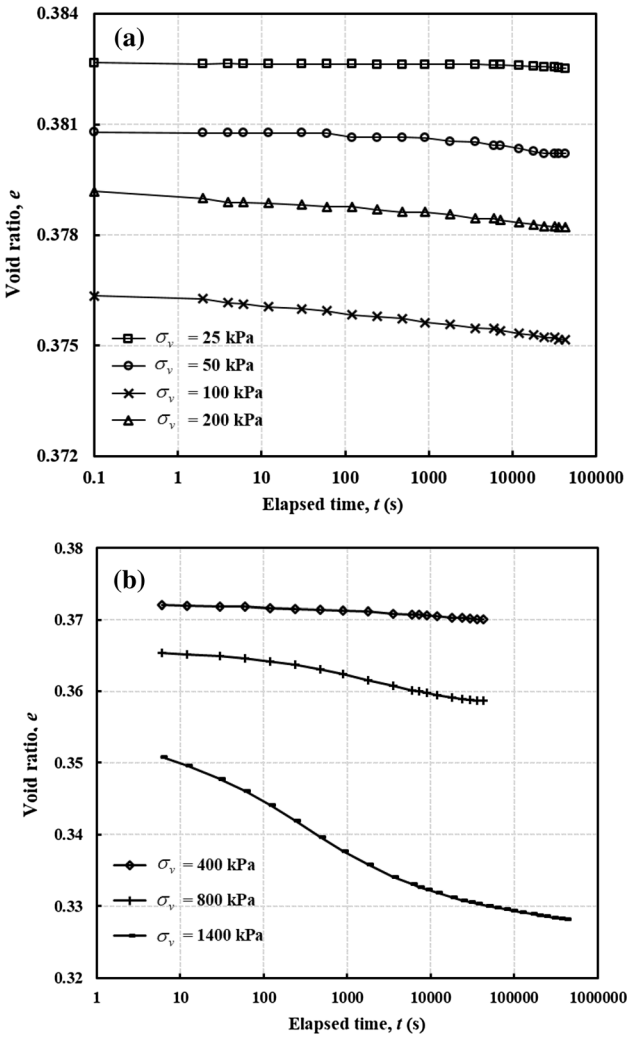


**Fig. 7** Plots of void ratio versus elapsed time (logarithmic scale) under 200 kPa matric suction when **a** $\sigma_v$ is lower than 400 kPa and **b** $\sigma_v$ is equal to and higher than 400 kPa

increase in the loading. For a loading smaller than 400 kPa (see Fig. 7a), the change in the void ratio is nearly linear with time. However, for a loading equal to or higher than 400 kPa (see Fig. 7b), the void ratio decreases nonlinearly with time. This difference is possibly explained by the compression mechanism in the particle perspective. Under a low load, the particle contact between two soil grains remains intact owing to particle friction, and transfers the load effectively; hence, not much variation occurred in the void ratio. At high-stress conditions, the frictional resistance between soil particles may not be sufficient to keep the soil particles intact; hence, the sliding or even breakage of soil grains could occur, thus leading to the rearrangement of the soil fabric and considerable reduction in the void ratio. As shown in Fig. 7b, under the total vertical loadings of 800 kPa and 1400 kPa, the primary consolidations are ended as reversed "S" turning points at

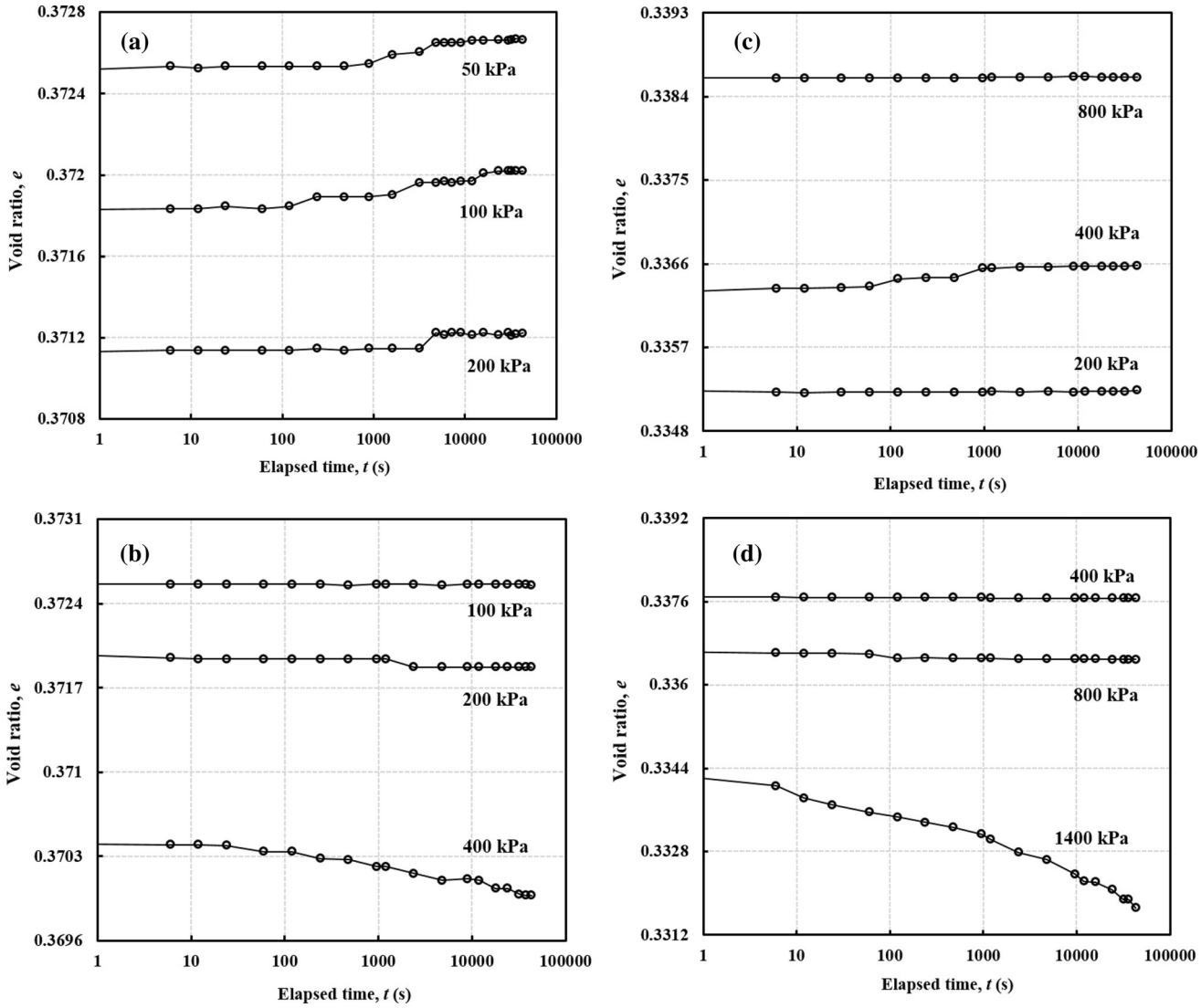


**Fig. 8** Plots of void ratio versus the elapsed time (logarithmic scale) on the two unloading–reloading loops under the matric suction of 200 kPa when: **a** $\sigma_v$ is unloaded from 400 to 50 kPa, **b** $\sigma_v$ is reloaded from 50 to 400 kPa, **c** $\sigma_v$ is unloaded from 1400 to 200 kPa, and **d** $\sigma_v$ is reloaded from 200 to 1400 kPa

approximately 2000s (33 min or 0.56 h). This is typical for most soils [63, 64]. The "S" turning points are not shown clearly for other curves as the soil specimens were over-consolidated. It is speculated that, after the previous equilibration of matric suction, the state of the tested soil is similar to "extremely dry clays" and "clay dry of optimum" [3] in which water tightly adheres to the soil particles, and air is the only fluid to flow from the tested soil. The air phase is relatively insensitive to the loading applied to the specimen because of its high compressibility [25].

The variation in void ratio versus the logarithm of time on the two unloading–reloading loops is presented in Fig. 8. It is also noteworthy, that, in this figure, the change in void ratio is approximately independent of time if the vertical loading is smaller than the preconsolidation stress, regardless of the unloading or reloading conditions. This proves the significance of the high stress used in the compaction for controlling the settlement.

Figure 9 depicts the variation in curves for the void ratio and effective vertical loading, $\sigma_v'$, under different matric suctions. The effective preconsolidation stresses ($\sigma_{vp}'$) were determined by the interception point of two fitting curves, as shown in the figure. The compression index ($C_c$), and the unloading–reloading index ($C_{r1}$, $C_{r2}$) represent the slopes of their corresponding fitting curves using the following equation:

$$C_c \text{ or } C_{ri(i=1,2)} = -\frac{\mathrm{d}(e)}{\mathrm{d}[\log(\sigma_v')]} \tag{9}$$

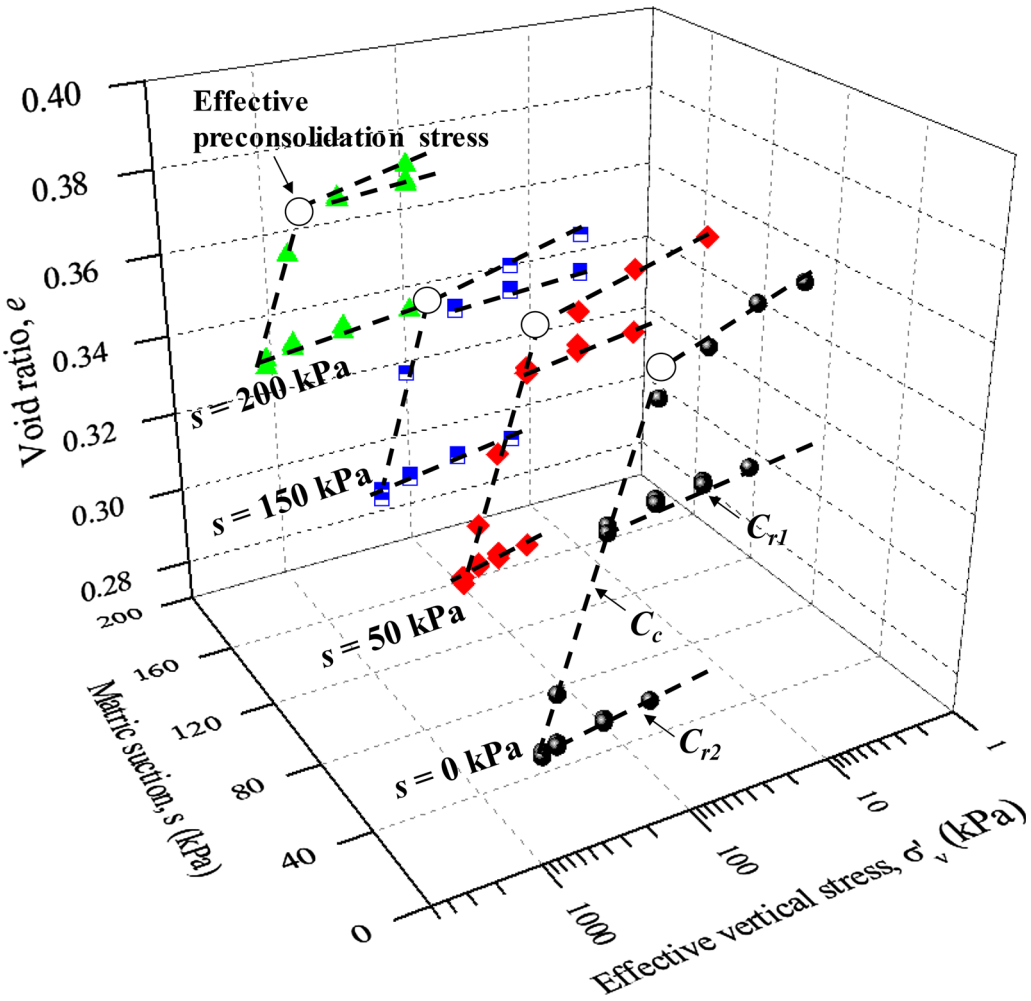


**Fig. 9** Plots of void ratio versus various effective vertical stresses under different matric suctions

The relationships between these parameters and matric suction are shown in Fig. 10. It is noteworthy that the matric suction improves the compression resistance of the soil significantly. Sharma [51] explained that the underlying reasons are (a) the additional normal force at the particle contacts applied by matric suction, and (b) the meniscus water at particle contacts preventing the slippage of particle and hence plastic deformation. As shown in Fig. 10a, the effective preconsolidation stress increases rapidly from 218.7 to 531.1 kPa when the matric suction increases from 0 kPa to 100 kPa. Further, the effective preconsolidation stress gains slightly by 60.9 kPa when the matric suction increases from 100 to 200 kPa. Figure 10b shows that $C_c$ increases with matric suction at a higher increasing rate at a low matric suction (0–100 kPa) and tends to stabilize when s is larger than 100 kPa. These show that any changes in the matric suction above 100 kPa has minimal effect on the compressibility characteristics of the soil. This trend between compression index and matric suction confirms with those reported in many studies [21, 22, 28, 46, 52]. However, other researchers have indicated that the compression index had an insignificant relationship with matric suction [17, 27, 44], or even decreased with increasing matric suction [12, 50, 59]. This disparity may be attributed primarily to the soil mineralogy, particle size distribution, stress range under consideration, and duration of applied loading. In terms of practical application, the determination of compression index should be customized for each specific case. In Fig. 10c, $C_{r1}$ decreases significantly from the value of 0.0055–0.0019 (i.e., 65.5%) as the matric suction is increased from 0 to 200 kPa. However, $C_{r2}$ is relatively insensitive to the matric suction and increases marginally with the increase in matric suction from 0 to 50 kPa, and subsequently decreases by 27.39% when the matric suction changes from 50 to 200 kPa. The increase in matric suction is expected to increase the stiffness of soil such that less void ratio change would occur if the effective vertical stress changes by the same amount. Nonetheless, if the

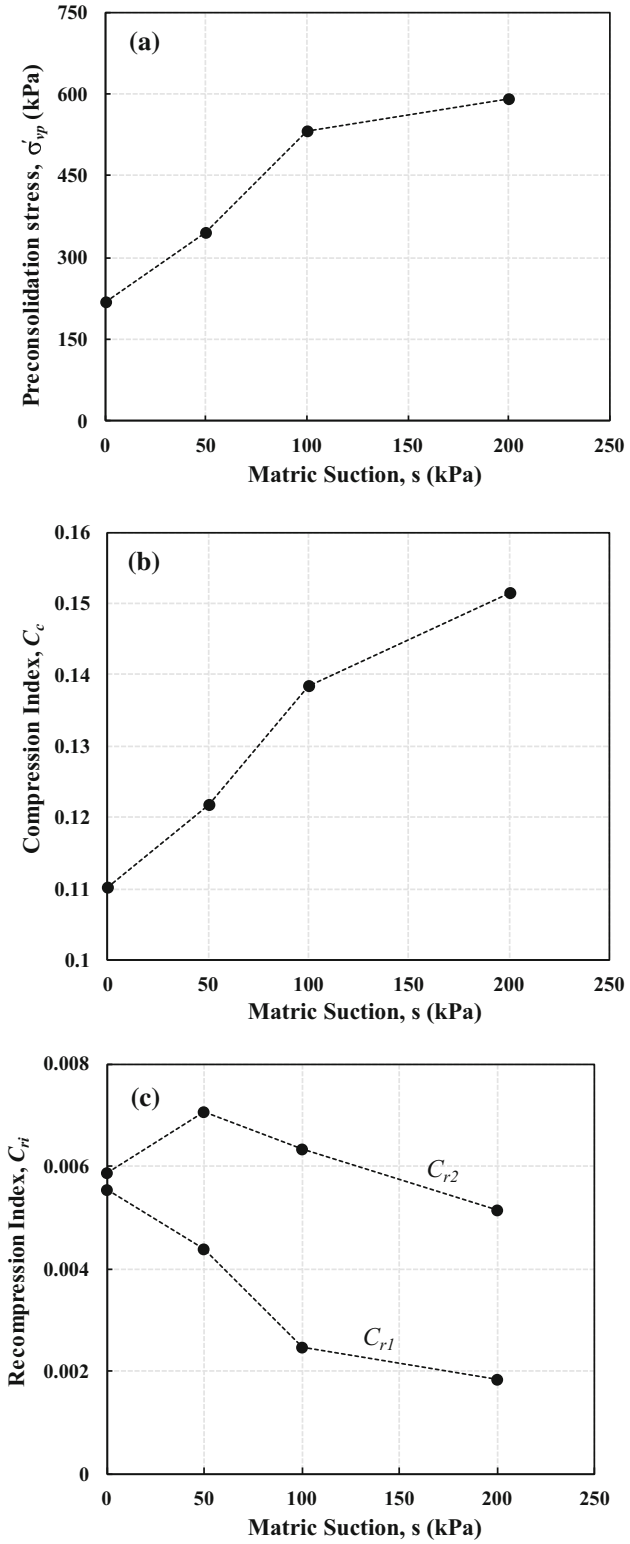


**Fig. 10** **a** Plot of preconsolidation stress versus matric suction; **b** plot of compression index versus matric suction; and **c** plots of unloading–reloading index versus matric suction

vertical loading is sufficiently large to cause a significant change to the soil structure, the effect of matric suction on the stiffness of soil becomes relatively small. It is reasonable to assume that the change in matric suction has no significant influence on the stiffness of the soil under a high-level stress state.

### 3.3 Time-dependent compression

Figure 11 shows the comparison of the time-dependent compression behavior with the different matric suctions under a specific total vertical loading. The curves of the time-dependent compression of the soils under different total vertical loadings and matric suctions were found to be divided into two types: (a) the relationship between time (log scale) and the change in void ratio is linear, which is termed as Type I; (b) the relationship between time (log scale) and change in void ratio is nonlinear, which is named as Type II. For the lower loading ranges (e.g., 50 kPa and 200 kPa), the slopes of log (time) versus the change in void ratio decreases with matric suction, and the curves resemble Type I curves. For the applied intermediate loading ranges (400 kPa), the curve is Type II under lower suctions (e.g., 50 kPa), whereas at higher suctions (i.e., greater than 50 kPa), the curve is similar in trend to that of Type I curves. Finally, for a larger vertical loading (800 kPa), the slope of log (time) versus the change in void ratio decreases with matric suction, and the curves resemble those of Type II. It is noteworthy that the time-dependent compression occurs when the vertical loading is lower than the preconsolidation stress.

The value of the time-dependent coefficient, $C_t$, can be obtained using the experimental data by the following:

$$C_t = -\frac{\Delta e}{\log(t/t_0)} \tag{10}$$

where $t_0$ correspond is the end of the transient period, and is 100 min in this study; $\Delta e$ is the change in void ratio from time $t_0$.

Figure 12 shows the linear relationship of $C_t$ against the effective vertical stress under one specific matric suction. Lai et al. [32] and McDowell [39] also observed the same trend when they investigated the creep behavior of the granular material and unsaturated landslide soils, respectively. In comparison, the values of $C_t$ are approximately constant or decrease with increased effective vertical stress for soft clays [34, 41, 68]. Furthermore, the increase in matric suction is found to decrease the time-dependent compression. However, the values of $C_t$ under a 100 kPa suction are close to those for a suction of 200 kPa, indicating that if any further increase occurs in the suction values above 200 kPa, a marginal decrease in $C_t$ may occur. This observation is in agreement with that of

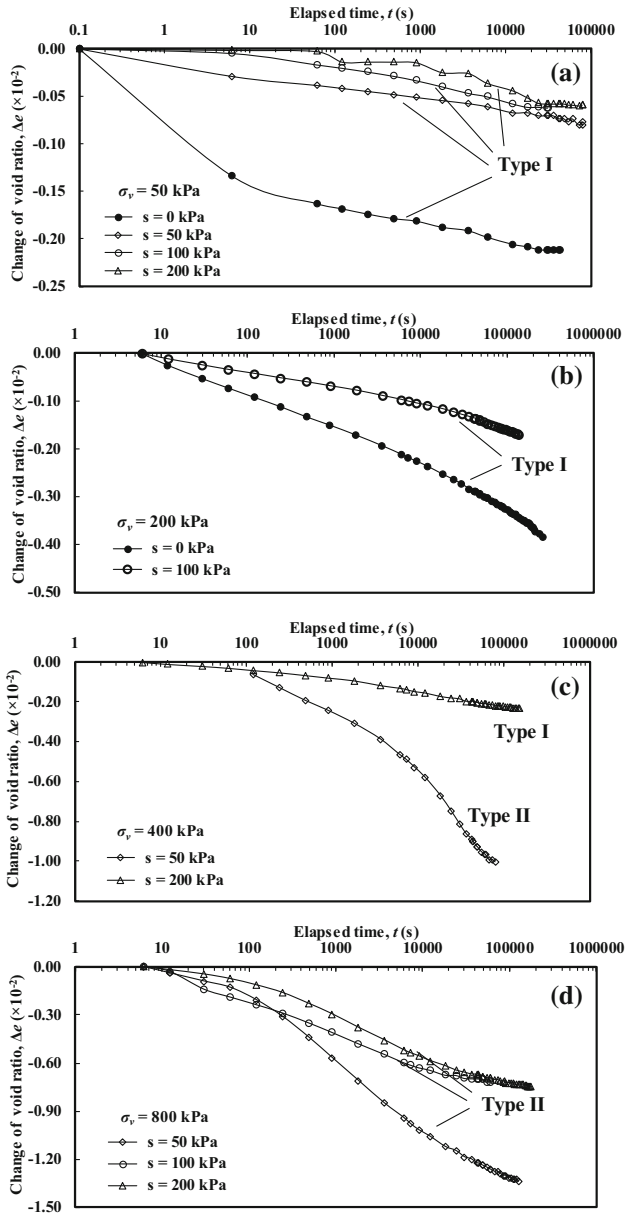


**Fig. 11** Change of void ratio with time of the fill under different vertical normal loading of **a** 50 kPa; **b** 200 kPa; **c** 400 kPa; and **d** 800 kPa with different suctions

agricultural soils [31]. The relationship between $C_c$ and $C_t$ is plotted in Fig. 13. The ratio, $C_t/C_c$, is typically adopted to analyze their correlation [41, 42]. Based on the experimental data, the best fitting value of $C_t/C_c$ is 0.023, which is close to the constant value (0.02) suggested by Oldecop and Alonso [48]. Further, 0.023 is used in the time-dependent model proposed by Oldecop and Alonso [48] to analyze the experimental results.

Based on the compression behavior of coarse-grained soil used in this study, a linear relationship (*y*-intercept equal to zero) is proposed between the creep coefficient and normalized effective vertical loading as follows:

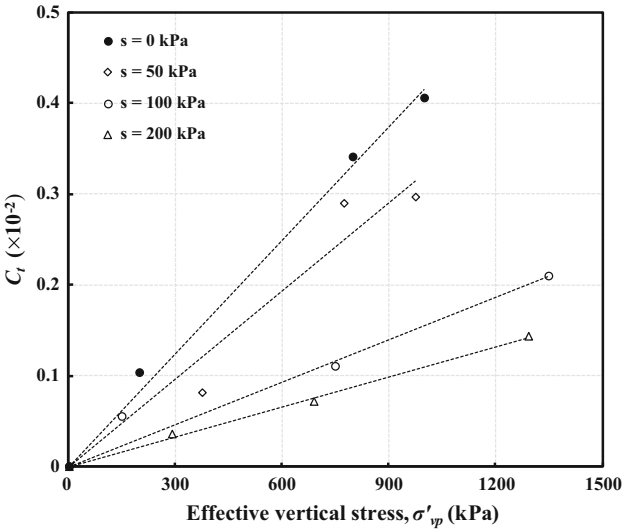


**Fig. 12** Relations of time-dependent compression coefficient, $C_t$, and effective vertical stress, $\sigma'_{vp}$, for different matric suctions

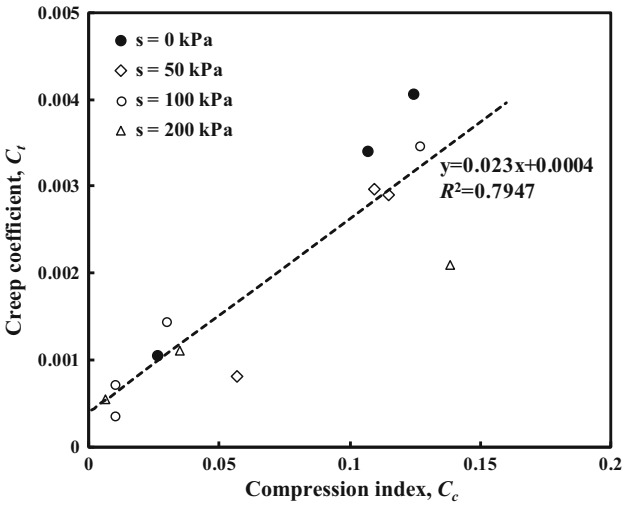


**Fig. 13** Relations of creep coefficient and compression index under four suction values

$$C_t = a \times \frac{\sigma'_v}{\sigma'_{vp}} \tag{11}$$

where $a$ is the fitting parameter. The effect of matric suction could be considered by adopting different preconsolidation stresses, $\sigma'_{vp}$. Furthermore, as shown in Fig. 14, the normalization ratio of $\sigma'_v/\sigma'_{vp}$ could capture the phenomenon where the time-dependent compression coefficient increases linearly with stress level [35, 39], and reflect the influence of matric suction. Equation (11) is relatively easy to be used for establishing the time-dependent compression behavior, and it is valid when the vertical

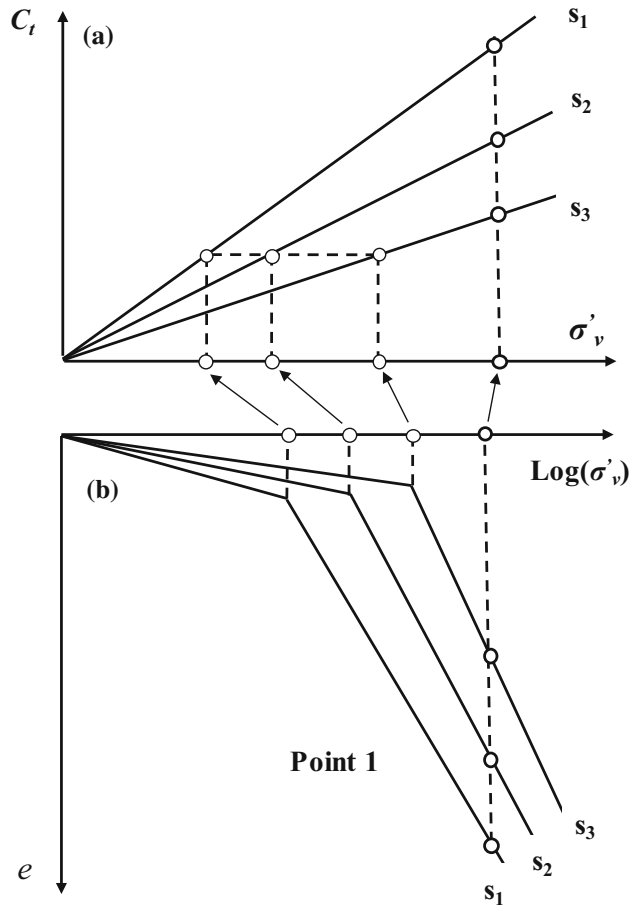


**Fig. 14** Conceptual illustration of creep coefficient and normalized vertical effective stress

loading is smaller than the preconsolidation stress. Figure 15 shows the relationship of $\sigma'_v / \sigma'_{vp}$ and $C_t$ based on the experimental results under different matric suctions. The value of $R^2$ is 0.9349, indicating the linear fitting is suitable for the coarse-grained soil utilized in this study.

The proposed Eq. (11) is verified by comparing the experimental data after 100 min using the values of $C_t$ obtained from the fitting equation. Furthermore, the model proposed by Oldecop and Alonso [48] was also used for comparison by adopting the value of $n$ = 1/0.023 (i.e., 43.48). The comparison results are shown in Fig. 16. The results from the proposed model match very well with the experimental data as compared to the analytical model proposed by Oldecop and Alonso [48], in which $C_t/C_c$ was oversimplified as a constant. However, it is noteworthy that this linear relationship between the normalized ratio of $\sigma'_v / \sigma'_{vp}$ and $C_t$ would only be valid within a certain stress range.

Further, the limitation of the model by Oldecop and Alonso [48] was that the settlement was infinite when the time was infinite. To overcome this limitation, a nonlinear function proposed by Yin [63] was adopted to describe the time-dependent compression:

$$\Delta\varepsilon_c = \frac{\psi'_0 \ln[(t+t_0)/t_0]}{1 + (\psi'_0/\Delta\varepsilon_l)\ln[(t+t_0)/t_0]} \tag{12}$$

where $\Delta\varepsilon_c$ is the time-dependent strain, $\psi'_0$ is a constant parameter, $\Delta\varepsilon_l$ is the limit of vertical strain, $t$ is the time from the end of primary consolidation, and $t_0$ is a constant parameter, which is typically assumed as the time at the end of the primary consolidation. When $t$ increases to infinity, $\Delta\varepsilon_c$ will approach $\Delta\varepsilon_l$ such that the limitation of the model by Oldecop and Alonso [48] can be avoided. If the compression is presented by the change in void ratio, subsequently Eq. (12) can be expressed as follows:

$$\Delta e_t = -\frac{C_t^0 \log[(t+t_0)/t_0]}{1 - (C_t^0/\Delta e_l)\log[(t+t_0)/t_0]} \tag{13}$$

where $\Delta e_t$ is the void ratio change after the end of the primary consolidation, $\Delta e_l$ is the creep limit of void ratio, and $C_t^0 = \psi'_0 \cdot V \cdot \ln(10)$. It is noteworthy that $C_t$ can be expressed as:

$$C_t = \frac{C_t^0}{1 - (C_t^0/\Delta e_l)\log[(t+t_0)/t_0]} \tag{14}$$

This indicates that $C_t$ is no longer a constant but decreases with time, $t$. In this study, $t_0$ is chosen as 900 s. Equation (13) can be written as follows:

$$\frac{\log[(t+t_0)/t_0]}{\Delta e_t} = -\frac{1}{C_t^0} + \frac{1}{\Delta e_l}\log[(t+t_0)/t_0] \tag{15}$$

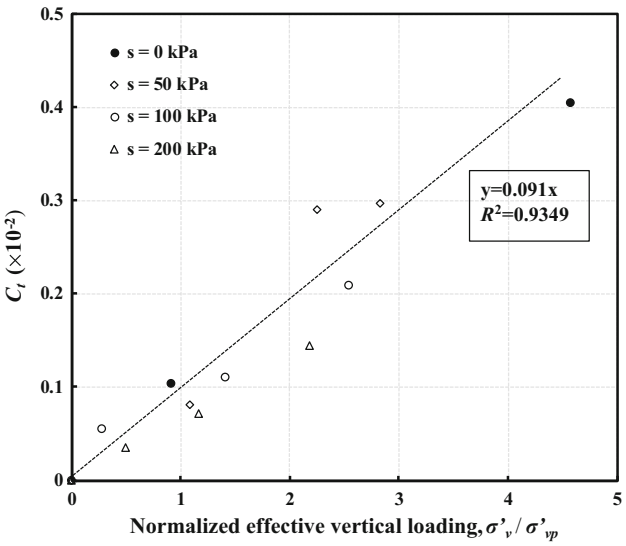


**Fig. 15** Correlation of creep coefficient to normalized vertical effective stress for all suctions

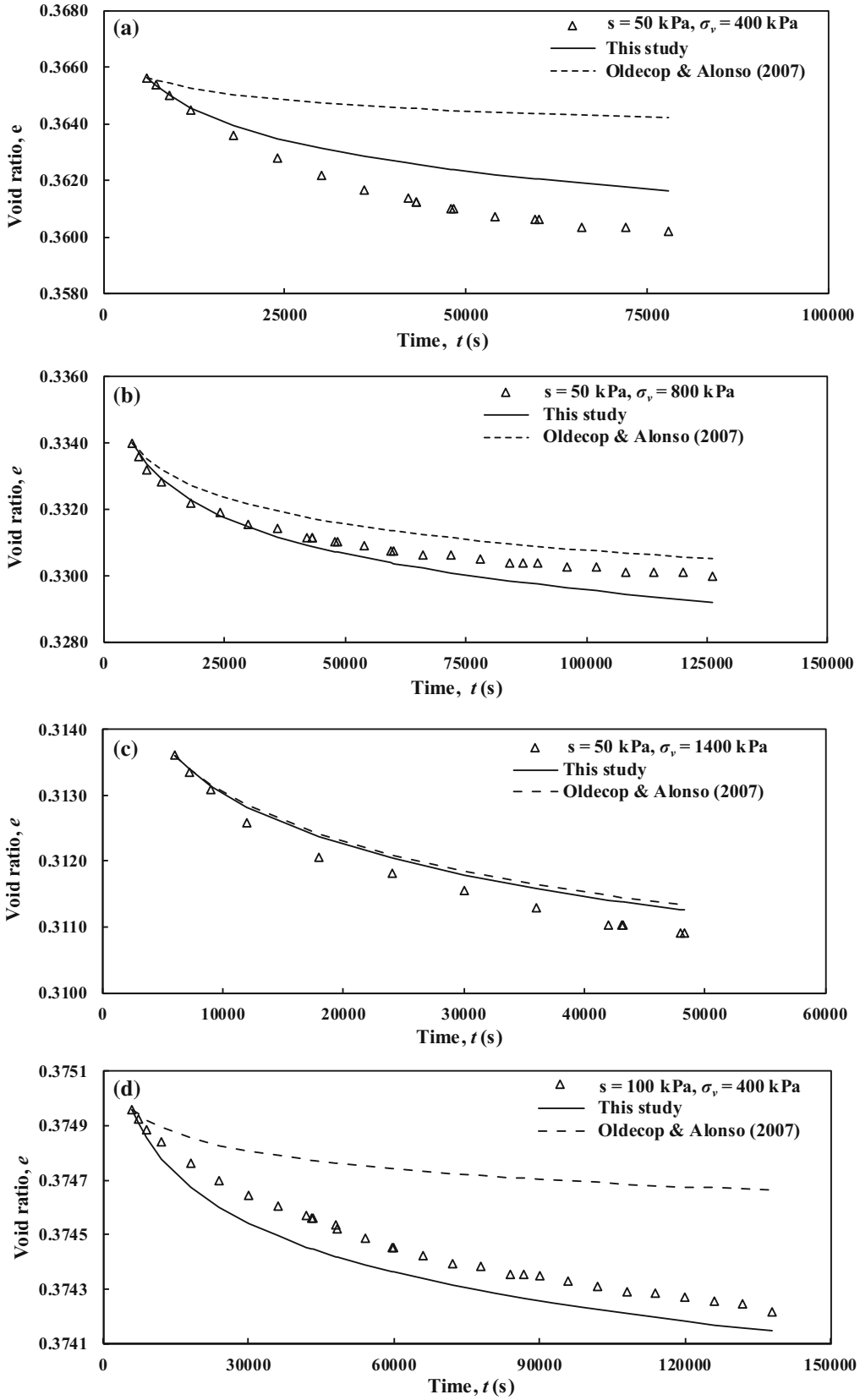


**Fig. 16** Comparison of experimental data and calculated results from Oldecop and Alonso [48] and the predicted $C_t$ using Eq. (11) under various stress states

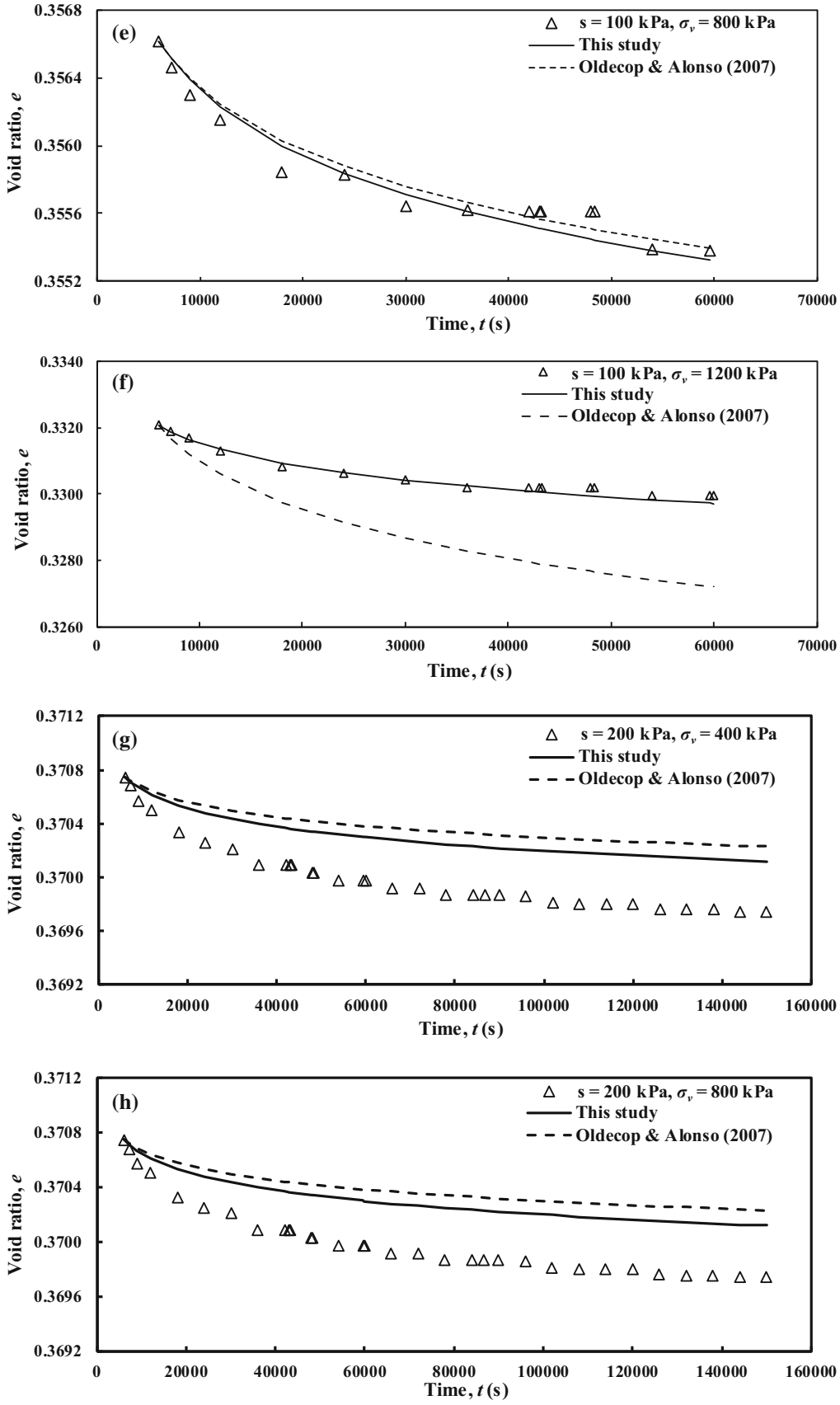


**Fig. 16** continued

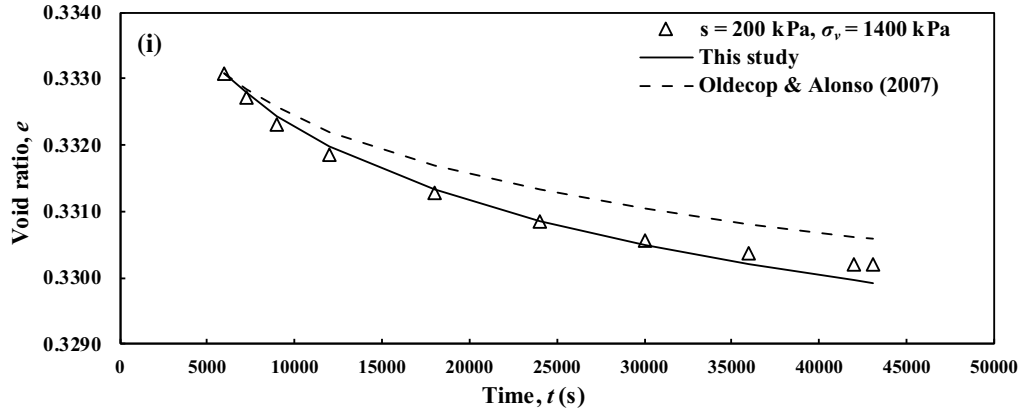


**Fig. 16** continued

Additionally, Yin [63] reported that this model is not suitable for fitting the unloading–reloading data because the creep on unloading or reloading is not significant. Hence, Eq. (15) was used to fit the data of every creep tests on the normal consolidation line (i.e., the effective vertical

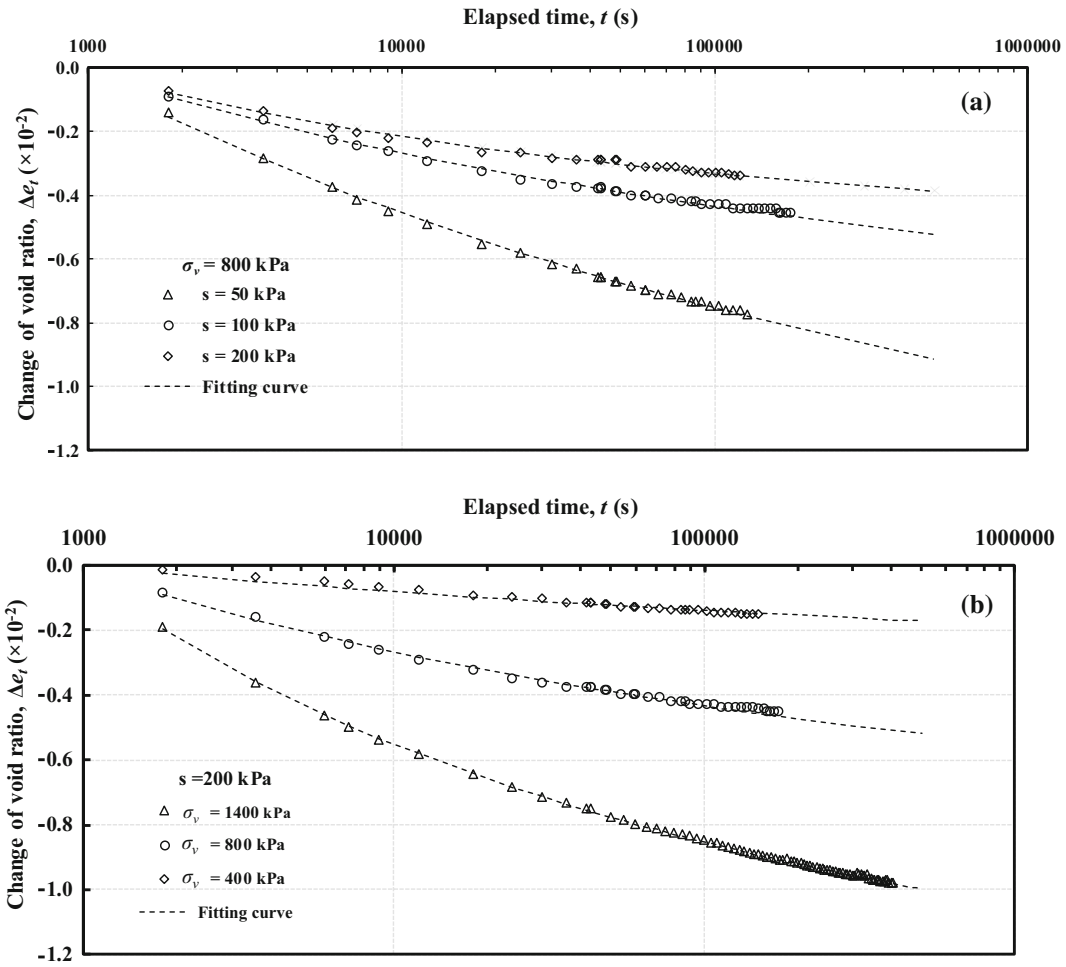


**Fig. 17** **a** Plot of the change of void ratio versus the elapsed time (logarithmic scale) when the total vertical stress is 800 kPa and under three levels of matric suction, and the fitting curves; **b** plot of the change of void ratio versus the elapsed time (logarithmic scale) when the matric suction is 200 kPa and under three total vertical stresses, and the fitting curves

**Table 3** Values of $C_t^0$ and $\Delta e_l$ under various stress states

| Matric suction, $s$ (kPa) | Vertical loading, $\sigma_v$ (kPa) | $C_t^0$ | $\Delta e_l$ |
|---|---|---|---|
| 50 | 800 | 0.00536 | − 0.0239 |
| | 1000 | 0.00271 | − 0.0076 |
| 100 | 800 | 0.00323 | − 0.0126 |
| | 1200 | 0.00530 | − 0.0109 |
| 200 | 800 | 0.00286 | − 0.0076 |
| | 1400 | 0.00749 | − 0.0170 |

loading is larger than the effective preconsolidation stress); subsequently, the values of $C_t$ and $\Delta e_l$ were determined and presented in Table 3. Figure 17a presents the data of creep tests under the total vertical loading of 800 kPa and three levels of matric suction. In Fig. 17b, under the same level of suction, the compression increases with increasing vertical loading. The fitting curves were plotted using each set of $C_t^0$ and $\Delta e_l$ for each stress condition. All the fitting curves were in good agreement with the test data, thus indicating that the proposed model is promising for predicting the development of creep compression. Nonetheless, it would be interesting to establish a generalized fitting model for predicting creep under all the stress states by conducting further tests.

## 4 Conclusions

In this study, the relationship between the effective stress parameter and matric suction was established using the data from a series of unsaturated drained triaxial tests. The influence of matric suction on consolidation and time-dependent compression behavior of coarse-grained soil was examined using a newly designed suction-controlled oedometer apparatus that enabled the accurate measurement of volumetric change of the specimens. Four suction-controlled oedometer tests were conducted on the soil specimens. The key findings from the laboratory tests under various stress state variables are as follows:

a. The compressibility of the soil fabric and the variation in void ratio with respect to time was directly proportional to the vertical loadings. Particularly, at a higher loading, the void ratio varied nonlinearly with time probably due to particle breakage and particle rearrangement.
b. The compression index and effective preconsolidation stress increased significantly when the specimen was changed from saturated to unsaturated. No obvious relationship between the unloading–reloading index and matric suction was observed if the specimen rebounded from a high level of stress.
c. A linear relationship between normalized effective vertical loading and time-dependent compression coefficient was proposed based on the experimental data. The time-dependent compression coefficients predicted by the linear relationship were used to predict the time-dependent compression behavior of the coarse-grained soil under different matric suctions, and indicated a better match as compared to the analytical model proposed by Oldecop and Alonso [48].
d. The nonlinear function proposed by Yin [63] was utilized to describe the experimental data. The nonlinear function could well predict the development of time-dependent compression of unsaturated coarse-grained materials.

**Acknowledgements** The authors acknowledge the financial supports from Research Institute for Sustainable Urban Development of The Hong Kong Polytechnic University (PolyU). The work in this paper is also supported by a National State Key Project "973" Grant (Grant No.: 2014CB047000) (Sub-project No. 2014CB047001) from Ministry of Science and Technology of the People's Republic of China, a CRF Project (Grant No.: PolyU12/CRF/13E) from Research Grants Council (RGC) of Hong Kong Special Administrative Region Government of China. The authors are also sincerely grateful to the reviewers for their constructive review comments.

## References

1. ASTM D 2487-06 (2006) Standard practice for classification of soils for engineering purposes (unified soil classification system). Annual Book of ASTM Standards, ASTM International, West Conshohocken, PA
2. ASTM D 5298-16 (2016) Standard test method for measurement of soil potential (suction) using filter paper. Annual Book of ASTM Standards, ASTM International, West Conshohocken, PA
3. Barden L (1965) Consolidation of compacted and unsaturated clays. Géotechnique 15(3):267–286
4. Bishop AW (1959) The principle of effective stress. Tek Ukebl 106(39):859–863
5. Bishop AW, Blight GE (1963) Some aspects of effective stress in saturated and partly saturated soils. Géotechnique 13(3):177–197
6. Borana L, Yin JH, Singh DN, Shukla SK (2015) A modified suction controlled direct shear device for testing unsaturated soil and steel plate interface. Mar Georesour Geotechnol 33(4):289–298
7. Borana L, Yin JH, Singh DN, Shukla SK (2016) Interface behavior from suction-controlled direct shear test on completely decomposed granitic soil and steel surfaces. Int J Geomech 16(6):D4016008
8. Borana L, Yin JH, Singh DN, Shukla SK (2017) Influence of matric suction and counterface roughness on shearing behavior of completely decomposed granitic soil and steel interface. Indian Geotech J 47(2):150–160
9. Borja RI (2004) Cam-Clay plasticity. Part V: a mathematical framework for three-phase deformation and strain localization analyses of partially saturated porous media. Comput Methods Appl Mech Eng 193:5301–5338

10. BS 1377 (1990) Methods of test for soils for civil engineering purpose. British Standards Institution, London
11. Burland JB (1967) Deformation of soft clay. Ph.D. thesis, Cambridge University, Cambridge
12. Chen ZH, Fredlund DG, Julian KMG (1999) Overall volume change, water volume change, and yield associated with an unsaturated compacted loess. Can Geotech J 36(2):321–329
13. Chen WB, Yin JH, Feng WQ (2018) A new double-cell system for measuring volume change of a soil specimen under monotonic or cyclic loading. Acta Geotech. https://doi.org/10.1007/s11440-018-0629-6
14. Chen WB, Yin JH, Feng WQ, Borana L, Chen RP (2018) Accumulated permanent axial strain of a subgrade fill under cyclic high-speed railway loading. Int J Geomech 18(5):04018018
15. Chen WB, Feng WQ, Yin JH, Borana L, Chen RP (2019) Characterization of permanent axial strain of granular materials subjected to cyclic loading based on shakedown theory. Constr Build Mater 198:751–761
16. Coop MR (1990) The mechanics of uncemented carbonate sands. Géotechnique 40(4):607–626
17. Cui K, Défossez P, Cui YJ, Richard G (2010) Quantifying the effect of matric suction on the compressive properties of two agricultural soil using an osmotic oedometer. Geoderma 156(3–4):337–345
18. Cui YJ, Delage P (1993) On the elasto-plastic behaviour of an unsaturated silt. ASCE Geotech Spec Publ 39:115–126
19. Fredlund DG, Morgenstern NR (1977) Stress state variables for unsaturated soils. J Geotech Eng Div 103(5):447–466
20. Fredlund DG, Xing A (1994) Equations for the soil-water characteristic curve. Can Geotech J 31(4):533–546
21. Futai MM, Almeida SS (2005) An experimental investigation of the mechanical behaviour of an unsaturated gneiss residual soil. Géotechnique 55(3):201–213
22. Gallipoli D, Gens A, Sharma R, Vaunat J (2003) An elasto-plastic model for unsaturated soil incorporating the effects of suction and degree of saturation on mechanical behavior. Géotechnique 53(1):123–135
23. Gan JKM, Fredlund DG, Rahardjo H (1988) Determination of the shear strength parameters of an unsaturated soil using the direct shear test. Can Geotech J 25(3):500–510
24. Hardin BO (1985) Crushing of soil particles. J Geotech Geoenviron ASCE 111(10):1177–1192
25. Ho DYF, Fredlund DG (1982) Strain rates for unsaturated soil shear strength testing. In: Proceedings of the seventh Southeast Asian geotechnical conference Hong Kong, vol 1, pp 787–803
26. Hossain MA, Yin JH (2010) Behavior of a compacted completely decomposed granite soil from suction controlled direct shear tests. J Geotech Geoenviron 136(1):189–198
27. Imhoff S, Da Saliva AP, Fallow D (2004) Susceptibility to compaction, load support capacity and soil compressibility of Hapludox. Soil Sci Soc Am J 68(1):17–24
28. Jotisankasa A, Ridley A, Coop M (2007) Collapse behavior of compacted silty clay in suction-monitored oedometer apparatus. J Geotech Geoenviron 133(7):867–877
29. Khalili N, Khabbaz MH (1998) A unique relationship for $\chi$ for the determination of the shear strength of unsaturated soils. Géotechnique 48(5):681–687
30. Khalili N, Geiser F, Blight GE (2004) Effective stress in unsaturated soils: review with new evidence. Int J Geomech 4(2):115–126
31. Koliji A, Laloui L, Vulliet L (2009) Behaviour of unsaturated aggregated soil in oedometric condition. Soil Found 49(3):369–380
32. Lai XL, Wang SM, Ye WM, Cui YJ (2014) Experimental investigation on the creep behavior of an unsaturated clay. Can Geotech J 51(6):621–628
33. Le TM, Fatahi B, Khabbaz H (2012) Viscous behavior of soft clay and inducing factors. Geotech Geol Eng 30(5):1069–1083
34. Leroueil S, Kabbai M, Tavenas F, Bouchard R (1985) Stress–strain–strain rate relation for the of sensitive natural clays. Géotechnique 35(2):159–180
35. Leung CF, Lee FH, Yet NS (1997) The role of particle breakage in pile creep in sand. Can Geotech J 33(6):888–898
36. Liu K, Chen WB, Feng WQ, Yin JH (2018) Experimental study on the unsaturated behavior of a compacted soil. In: The 7th international conference on unsaturated soils (UNSAT2018), Hong Kong, China
37. Marsal RJ (1967) Large scale testing of rockfill materials. J Soil Mech Found Div 93(2):27–43
38. Marsal RJ, Arellano LR, Guzmán MA, Adame H (1976) El Infiernillo. In behavior of dams built in Mexico. UNAM México: Instituto de Ingeniería, pp 239–312
39. Mcdowell GR (2003) Micromechanics of creep of granular materials. Géotechnique 53(10):915–916
40. Mcdowell GR, Bolton MD (1998) On the micromechanics of crushable aggregates. Géotechnique 48(5):667–679
41. Mesri G, Paul MG (1977) Time-and stress-compressibility interrelationship. J Geotech Geoenviron 103(5):417–430
42. Mesri G, Feng TW, Benak JM (1990) Postdensification penetration resistance of clean sands. J Geotech Eng 116(7):1095–1115
43. Mesri G, Vardhanabhuti B (2009) Compression of granular materials. Can Geotech J 46(2):369–392
44. Mosaddeghi MR, Hemmat A, Hajabbasi MA, Vafaeian M, Alexandrou A (2006) Plate sinkage versus confined compression tests for in situ soil compressibility studies. Biosyst Eng 93(3):325–334
45. Mountassir GE, Sánchez M, Romero E (2014) An experimental study on the compaction and collapsible behavior of a flood defence embankment fill. Eng Geol 179:132–145
46. Mun W, McCartney JS (2015) Compression mechanisms of unsaturated clay under high stresses. Can Geotech J 52(12):2099–2112
47. Oldecop LA, Alonso EE (2001) A model for rockfill compressibility. Géotechnique 51(2):127–139
48. Oldecop LA, Alonso EE (2007) Theoretical investigation of the time-dependent behaviour of rockfill. Géotechnique 57(3):289–301
49. Pasha AY, Khoshghalb A, Khalili N (2015) Pitfalls in interpretation of gravimetric water content-based soil-water characteristic curve for deformable porous media. Int J Geomech 16(6):D4015004
50. Rampino C, Mancuso C, Vinale F (2000) Experimental behaviour and modelling of an unsaturated compacted soil. Can Geotech J 37(4):748–763
51. Sharma RS (1998) Mechanical behaviour of unsaturated highly expansive clays. Ph.D. thesis, University of Oxford, UK
52. Sheng DC (2011) Review of fundamental principles in modelling unsaturated soil behaviour. Comput Geotech 38:757–776
53. Shi XS, Herle I (2014) Laboratory investigation of artificial lumpy materials. Eng Geol 183:303–314
54. Shi XS, Herle I (2016) Analysis of the compression behavior of artificial lumpy composite materials. Int J Numer Anal Methods Geomech 40(10):1438–1453
55. Shi XS, Herle I (2017) Numerical simulation of lumpy soils using a hypoplastic model. Act Geotech 12(2):349–363
56. Shi XS, Herle I (2017) A model for natural lumpy composite soils and its verification. Int J Solids Struct 121:240–256

57. Shi XS, Herle I, Muir Wood D (2018) A consolidation model for lumpy composite soils in open-pit mining. Géotechnique 68(3):189–194
58. Sivakumar V (1993) A critical state framework for unsaturated soil. Ph.D. thesis, University of Sheffield, UK
59. Sun D, Sun W, Yan W, Li J (2010) Hydro-mechanical behaviours of highly compacted sand-bentonite mixture. J Rock Mech Geotech Eng 2(1):79–85
60. Vanapalli SK, Fredlund DG, Pufahl DE, Clifton AW (1996) Model for the prediction of shear strength with respect to soil suction. Can Geotech J 33(3):379–392
61. Wheeler SJ, Sivakumar V (1995) An elasto-plastic critical state framework for unsaturated soil. Géotechnique 45(1):35–53
62. Yao YP, Qi SJ, Che LW (2016) Computational method of post-construction settlement for high-fill embankments. J Hydroelectr Eng 35(3):1–10 **(in Chinese)**
63. Yin JH (1999) Non-linear creep of soils in oedometer tests. Géotechnique 49(5):699–707
64. Yin JH (1999) Properties and behaviour of Hong Kong marine deposits with different clay contents. Can Geotech J 36(6):1085–1095
65. Yin JH, Graham J (1989) Viscous–elastic–plastic modelling of one-dimensional time-dependent behaviour of clays. Can Geotech J 26(2):199–209
66. Yin JH, Graham J (1994) Equivalent times and elastic viscoplastic modelling of time-dependent stress-strain behaviour of clays. Can Geotech J 31(1):42–52
67. Yin JH, Zhu JG, Graham J (2002) A new elastic viscoplastic model for time-dependent behaviour of normally and overconsolidated clays: theory and verification. Can Geotech J 39(1):157–173
68. Yin ZY, Chang CS, Karstunen M, Hicher PY (2010) An anisotropic elastic–viscoplastic model for soft clays. Int J Solids Struct 47(5):665–677
69. Zhou WH, Xu X, Garg A (2016) Measurement of unsaturated shear strength parameters of silty sand and its correlation with unconfined compressive strength. Measurement 93:351–358